Coupled orientational and displacive degrees of freedom in the high-temperature plastic phase of the carbon tetrabromide α-CBr_4

Jacob C. W. Folmer,[1] Ray L. Withers,[2] T. R. Welberry,[2] and James D. Martin[1]
[1]*Department of Chemistry, North Carolina State University, Raleigh, North Carolina 27695-8204, USA*
[2]*Research School of Chemistry, Australian National University, Canberra, ACT, 0200, Australia*
(Received 22 August 2007; revised manuscript received 27 November 2007; published 10 April 2008)

Two-dimensional single-crystal synchrotron x-ray diffraction of the high-temperature plastic phase of CBr_4 reveals relatively sharp $\mathbf{G}\pm\frac{1}{2}\{110\}^*$ sheets of diffuse intensity (where **G** represents the set of average structure *Fm*-3*m* allowed Bragg reflections). This intense and highly structured diffuse scattering arises from the large amplitude excitation of transverse polarized displacive modes of distortion and shows that a set of six possible orientations of the individual CBr_4 molecules in the plastic phase are strongly coupled with displacive relaxational degrees of freedom. Using Monte Carlo simulations to model the diffuse intensity, the displacive relaxations are shown to be along the molecular nearest-neighbor $\frac{1}{2}\langle 110\rangle$ real space directions associated with the relative orientations of individual and nearest-neighbor CBr_4 tetrahedra.

DOI: 10.1103/PhysRevB.77.144205 PACS number(s): 61.05.C−, 61.43.Bn, 61.90.+d

I. INTRODUCTION

Liquids made up of globular molecules frequently crystallize on cooling from the melt into a soft, plastic, crystalline phase characterized by high symmetry (often cubic), low entropy of fusion, and a high degree of orientational and displacive disorder.[1–5] On cooling, there is often a further phase transition into a fully ordered, nonplastic crystalline phase. This low-temperature nonplastic polymorph generally adopts a lower symmetry and typically exhibits a large increase in mechanical strength.[2,3] The heavy orientational and displacive disorder characteristic of the plastic state means that such phases are characterized by average structure Bragg reflections, both few in number and weak in intensity, accompanied by a large amount of diffuse scattering.[6,7] The high-temperature cubic *Fm*-3*m*, $\mathbf{a}\sim 8.82-8.85$ Å, α form of carbon tetrabromide, CBr_4, is a prototypical plastic crystal.[8–15] It is reported to be stable between the melting point at ~366 K and ~320 K,[1,5,8], below which it undergoes a phase transition into a nonplastic monoclinic superstructure β form.[10] In the cubic plastic phase, only 16 nonzero Bragg reflections were detected initially[11] (in a later study this number was increased to 22[16]) of which only two (the 111 and 002) are relatively intense. In addition, "…an intense and rather broad diffuse scattering peak was observed near 2 $Å^{-1}$…" which could not be fitted over "…the range …$2.0\leqslant Q\leqslant\sim 3.0$ $Å^{-1}$…."[17] The modeling and qualitative understanding of the crystal chemical origin of this latter disorder is the major objective of the current paper.

The earliest and simplest picture of a plastic crystal envisaged that the constituent molecules would be sited close to the average structure lattice sites (fcc in this case), but rotating largely independently of one another to form molecular "spheres." Such a spherical approximation to what is inherently a tetrahedral molecule indeed appears to be appropriate for CD_4.[9] In the case of CBr_4 the deviation from a spherical shape is more important. Given an intramolecular C-Br distance of ~1.91 Å and an intermolecular Br-Br van der Waals radius of $\sim\frac{1}{2}\times 3.78$ Å,[10] the radius of a freely rotating CBr_4 sphere would be $r\sim 3.80$ Å. Thus, for molecules not to overlap along the nearest neighbor $\frac{1}{2}\langle 110\rangle$ directions of the fcc molecular lattice, $a=2\sqrt{2}r$ would need to be >10.75 Å, resulting in a volume 1.81 times the actual volume (i.e., about half the actual density) of the plastic α form and 1.94 times the volume of the low-temperature monoclinic β form. In the *Fm*-3*m* plastic crystalline phase, the CBr_4 molecules clearly have nowhere near enough room to rotate independently of one another. There must therefore be strong nearest-neighbor intermolecular orientational and associated displacive correlations.[12,16]

The nature and diffraction consequences of these nearest-neighbor correlations, however, are far from clear, i.e., if one particular CBr_4 molecule is locally in a particular orientation, what are the implications for the orientation and positioning of the nearest-neighboring CBr_4 molecules and how does this give rise to the observed structured diffuse scattering? This paper aims to address these questions using recently obtained highly structured x-ray diffuse scattering data obtained from α-CBr_4.

II. EXPERIMENTAL RESULTS

A. Methods

A sample of multiply sublimed CBr_4 (Ref. 18) was sealed in a 0.7 mm fused silica capillary and affixed to a goniometer on beam line X7B at the National Synchrotron Light Source (NSLS), Brookhaven National Laboratory. The line was equipped with a programmable forced air heater with temperature control of ±0.5°. Variable temperature diffraction experiments were performed to investigate the structural phase transitions between room temperature and 383 K (see Fig. 1). In a typical experiment, the sample was heated at a rate of 1°/min to 5°/min between room temperature and 383 K. Diffraction data were collected for 20 sec at regular intervals of 1 to 2 minutes. Oscillation photos were taken in Debye-Scherrer sample geometry using a MAR 345 image plate (IP) detector with a wavelength of 0.922 Å over an oscillation angle of 5° for each image. The wavelength, sample-to-detector distance, titling angle of the IP, and zero

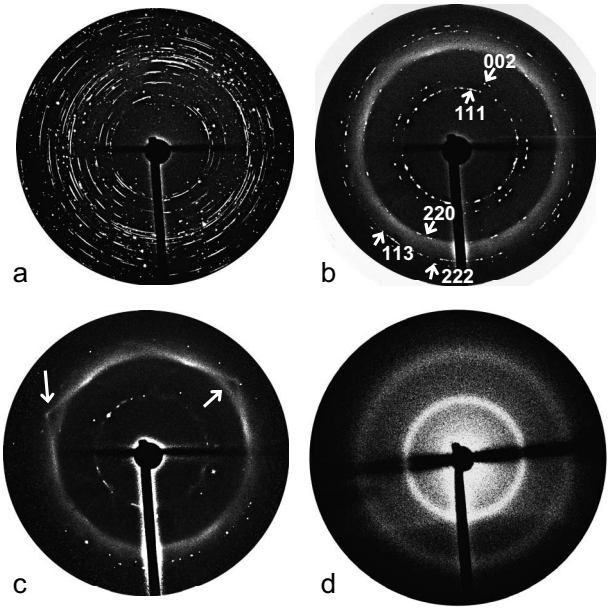

FIG. 1. Selected two-dimensional (2D) x-ray diffraction images collected while heating a sample of CBr_4 between room temperature and 383 K. (a) Room temperature (RT), (b) 323 K, (c) 358 K (arrows indicate sharp and circular diffuse patterns), (d) 378 K.

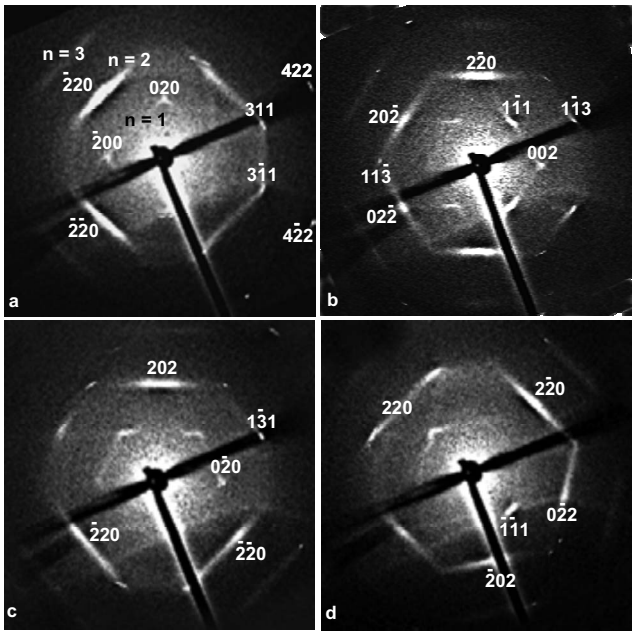

FIG. 2. Four rotation photographs of a near single plastic crystal of CBr_4 held at a 338 K isotherm after cooling from the melt. Each individual oscillation image is a 5° rotation angle image. (a) is taken fairly close to an ⟨001⟩ orientation, (b) is taken near the midway point between a ⟨110⟩ and a ⟨332⟩ orientation, (c) is taken tilted a further ~15° away from the [001] zone axis orientation relative to (a) around the $[020]^*$ reciprocal lattice direction, while (d) is taken tilted a few degrees away from a [112] zone axis orientation towards a [113] zone axis orientation (see the text for details).

shift position of the IP for the data collected were calibrated to a LaB_6 standard using the fit2d software package to analyze the full Debye-Scherrer rings of the MAR data.[19] Equivalent data were also collected on the X6B beam line at the NSLS using a SMART charge-coupled device (CCD) tuning the wavelengths (0.948–0.914 Å) across the Br K 1*s* absorption edge (13474 eV=0.920 Å).

Single plastic crystals were grown *in situ* by cooling the melt at a rate of about 1.5°/min. At an isotherm of 338 K the plastic crystal was evaluated with a series of 36 oscillation photographs in incremental steps of 5° over 180° of rotation. In this experiment it was not possible to predetermine the crystallographic orientation of the CBr_4 single crystal relative to the capillary (and hence incident x-ray beam). The rotation axis turned out not to be aligned with a high symmetry reciprocal lattice direction, but the 36 consecutive images ensure that reciprocal space was sufficiently sampled to characterize the highly structured diffuse intensity distribution of the plastic phase.

B. Temperature-dependent results

The structural phase transformations upon heating and cooling CBr_4 are apparent in the selected images from the variable temperature x-ray diffraction experiments shown in Figs. 1 and 2. At room temperature [see Fig. 1(a)] a quite polycrystalline pattern of the nonplastic β monoclinic phase is observed. On heating through the β to α phase transition (at ~320 K) to 323 K, the initially large number of discrete spotted diffraction rings characteristic of the nonplastic, monoclinic β phase disappear at the transformation to the plastic, cubic (Fm-3m) α phase [see Fig. 1(b)]. Five sharp polycrystalline (spotted) rings of the α plastic phase [the 111, 002, 220, 113, and 222 rings, respectively, labeled in Fig. 1(b)] are observed as well as a pronounced continuous ring of broad diffuse scattering, the inner radius of which falls on the 220 polycrystalline ring (at $Q=2\pi|\mathbf{g}|\sim 2.02$ Å^{-1}). It appears to extend virtually all the way out to the 113 polycrystalline ring (at $Q=2\pi|\mathbf{g}|\sim 2.37$ Å^{-1}). Diffuse scattering is also observed in the vicinity of the inner 111 and 002 polycrystalline rings but is very weak. The outer broad "ring" of intense diffuse scattering is clearly the same diffuse scattering that could not be modeled in the earlier neutron powder diffraction study of Dolling *et al.*, "…the agreement between theory and experiment is reasonably satisfactory except in the range …$2.0 \leqslant Q \leqslant \sim 3.0$ Å^{-1}…."[17] It is interesting to note that very early x-ray work on the plastic phase of CCl_4 also reported the same type of "…extremely heavy nonradial diffuse scattering…."[6] Upon further heating (or annealing time), the initially quite polycrystalline sample gradually anneals into larger and larger domains apparent in the form of a gradual "cannibalization" or disappearance of the original discrete diffraction spots and arcs [compare Figs. 1(b) and 1(c)]. At a temperature of 358 K [see Fig. 1(c)] the original ~2.0–2.4 Å^{-1} outer diffuse "ring" of Fig. 1(b) evolves into a quite structured sharp hexagonal shape [apparent only in the top half of Fig. 1(c)] on top of a slightly more diffuse circular ring shape [both arrowed in Fig. 1(c)]. Similar anisotropy is observed for the inner diffuse ring, but is less clear due to the weaker intensity. This evolution continues up to the melting point, beyond which point the pattern becomes isotropic and the inner diffuse ring becomes the most intense scatter-

ing feature [Fig. 1(d)]. From the crystallographic point of view, this represents the traditional characteristic signature of the plastic to liquid phase transition as pointed out by Dolling *et al.*,[17] "…when the (plastic) crystal melts, the intense (111) and (200) …peaks degenerate into the main "diffraction" peak of the liquid…." The sharp, inner diffuse scattering in the melt of CBr_4 is of innate importance as it is similar to that reported for a variety of tetrahedral molecular and network liquids.[20]

From differential scanning calorimetry (DSC) studies, Yoon[5] reported a melting transition temperature of 366.4 K, Staveley[1] a melting temperature of 363.3 K, and Silver and Rudman[8] a melting temperature of 367.4 K. They further stated "…it might not even be proper to speak of a sharp melting point… The soft, plastic nature of these phases suggest that it might be most practical to speak of a melting point range …It was decided to report the (reproducible) temperature at which melting is completed rather than the (variable) temperature at which pre-melting phenomena begin to occur…." Such comments and the observed variable temperature diffraction are consistent with the notion of a gradual loss of order preceding the melting transition.

Upon cooling from the melt, structured diffuse appears immediately on formation of the α phase. Cooling down to 338 K (and longer time in the plastic crystalline state) allows the capillary sample of CBr_4 to grow into nearly a single crystal of plastic α phase (Fig. 2). At this temperature, the intense, inner diffuse ring at ~ 1.2 Å^{-1} in the liquid state is replaced by much weaker highly structured diffuse patterns in the $Q \sim 1.2$ Å^{-1} portion of the pattern. The outer weak diffuse of the liquid, $Q \sim 2$ Å^{-1}, is replaced by the relatively more intense highly structured diffuse scattering. The fcc Bragg reflections for the cubic α phase are also observed.

C. Single crystal of the plastic phase

To characterize the highly structured diffuse scattering of α-CBr_4 a series of 36 oscillation photographs (5° oscillations over 180°) was taken of a near single plastic crystal held at a 338 K isotherm. Figure 2 shows four of the more symmetric individual oscillation images. Figure 2(a) is taken fairly close (at an estimated average orientation of ~8.5°) to an ⟨001⟩ orientation around the $[020]^*$ reciprocal lattice direction [see the relevant Ewald sphere construction shown in Fig. 3(b)], Fig. 2(b) is taken at an estimated average orientation of ~8.5° to a $[-1,-1,0]$ orientation around the $[2,-2,0]^*$ reciprocal lattice direction [see the relevant Ewald sphere construction shown in Fig. 4(b)], Fig. 2(c) is taken tilted a further 15° or so away from the [001] zone axis orientation relative to Fig. 2(a) around the $[020]^*$ reciprocal lattice direction while Fig. 2(d) is taken tilted a few degrees away from a [112] zone axis orientation towards a [113] zone axis orientation. While the images initially look similar to simple cross sections of reciprocal space, the relatively large curvature of the Ewald sphere ($K=1/\lambda=1.0846$ Å^{-1}) relative to the CBr_4 reciprocal lattice ($|\langle 002\rangle^*|=2/8.82-0.2268$ Å^{-1}; see, e.g., Figs. 3 and 4) ensures that such an interpretation is too simplistic. It will be shown below that such images can only be understood in terms of Ewald sphere cuts through

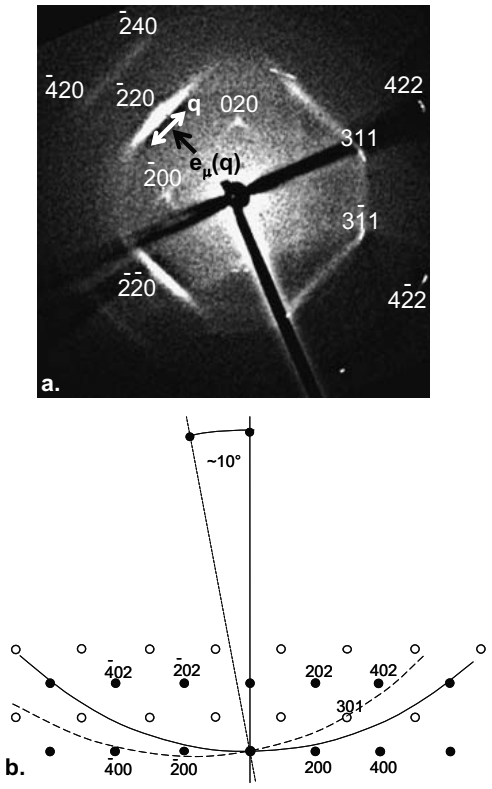

FIG. 3. (a) A 5° rotation angle image taken at an estimated average orientation of ~8.5° degrees to an ⟨001⟩ orientation around the $[020]^*$ reciprocal lattice direction. Diffuse streaking along the $[220]^*$ reciprocal lattice direction is marked by the doubled-headed arrow and the label **q** while the orthogonal directions of the atomic shifts responsible are labeled by the displacement eigenvector $\mathbf{e}_\mu(\mathbf{q})$ and the single-headed arrow. (b) A drawn to scale Ewald sphere construction of the $h0l^*$ plane of reciprocal space for an incident beam orientation along $[00,-1]$ (the solid Ewald sphere line) and tilted away from the $[00,-1]$ direction around the $[020]^*$ axis by $\phi \sim 10°$ (the dashed Ewald sphere line). The filled circles correspond to allowed Bragg reflections of the *Fm*-3*m* average structure while the open circles are not allowed by the face-centered lattice. Allowed reflections immediately above and below project onto the open circle positions shown (the projection direction is perpendicular to the drawing plane).

transverse polarized, $\frac{1}{2}\{-1,1,0\}^*$ sheets of diffuse scattering running through all allowed average structure Bragg reflections (see Fig. 5).

Consider, for example, the oscillation image shown in Fig. 3(a). On the right-hand side of this image, Bragg reflections such as $[311]^*$, $[3,-1,1]^*$, $[422]^*$, and $[4,-2,2]^*$ are clearly excited whereas on the left-hand side of the image the $[-2,0,0]^*$ Bragg reflection appears to be weakly excited along with very strong, transverse polarized (see below), $\mathbf{q} \sim \varepsilon[-2,2,0]^*$ and $\varepsilon[-2,-2,0]^*$ diffuse streaking running through, or very close to, the $\mathbf{G}=[-2,-2,0]^*$ and $[-2,2,0]^*$ Bragg reflections, respectively. The fact that such diffuse streaking is also present on the right-hand side of Fig. 3(a) (where the $[220]^*$ and $[2,-2,0]^*$ Bragg reflections are clearly not excited) shows that the diffuse running through the $\pm[220]^*$ and $\pm[2,-2,0]^*$ Bragg reflections is not localized to the $\varepsilon[220]^*$ and $\varepsilon[2,-2,0]^*$ directions but is rather

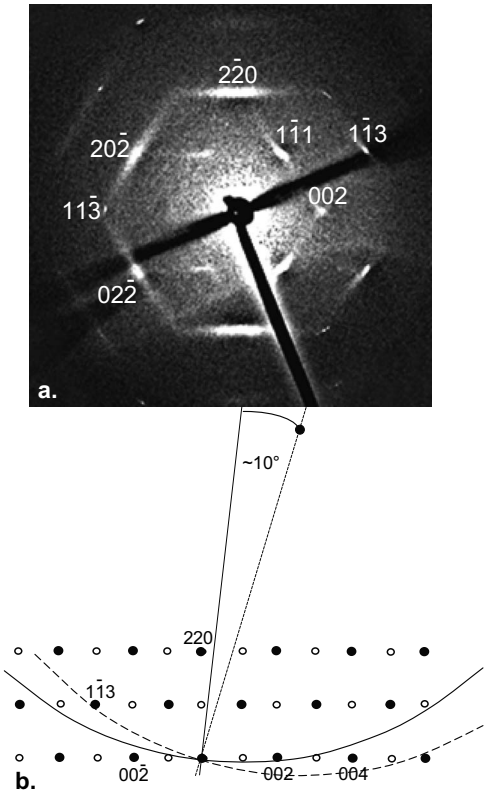

FIG. 4. (a) a 5° rotation angle image taken at an estimated average orientation of ~8.5° to a $[-1,-1,0]$ orientation around the $[2,-2,0]^*$ reciprocal lattice direction. (b) A drawn to scale Ewald sphere construction of the hhl^* plane of reciprocal space for an incident beam orientation tilted by 6.00° from the $[-1,-1,0]$ orientation around the $[2,-2,0]^*$ reciprocal lattice direction (the solid Ewald sphere line) and by ~15.26° from the $[-1,-1,0]$ orientation around the $[2,-2,0]^*$ reciprocal lattice direction (the dashed Ewald sphere line). The filled circles correspond to allowed Bragg reflections of the *Fm*-3*m* average structure while the open circles are not allowed by the face-centered lattice. Allowed fcc Bragg reflections immediately above and below project onto the open circle positions shown (the projection direction is perpendicular to the drawing plane).

part of essentially continuous $\frac{1}{2}(1,-1,0)^*$ and $\frac{1}{2}(110)^*$ sheets of diffuse intensity [parallel to the green shaded planes in Fig. 5(a) and corresponding lines in Figs. 5(b) and 5(c)]. Note that the $\mathbf{q}=\varepsilon[-2,-2,0]^*$ diffuse streaking running through the $[-200]^*$ and $[020]^*$ Bragg reflections in Fig. 3(a) [also light blue shaded regions in Fig. 5(a) and lines in Figs. 5(b) and 5(c)] automatically gives rise to $\mathbf{q}=\varepsilon[-2,-2,0]^*$ diffuse streaking running through, or very close to, the fcc forbidden $[-1,1,0]^*$ position of reciprocal space. Likewise the $\mathbf{q}=\varepsilon[-2,-2,0]^*$ diffuse streaking running through other allowed Bragg reflections such as $[-2,4,0]^*$ and $[-4,2,0]^*$ seen in Fig. 3(a) [see lavender shaded planes in Fig. 5(a) and lines in Figs. 5(b) and 5(c)] gives rise to diffuse $\mathbf{q}=\varepsilon[-2,-2,0]^*$ diffuse streaking running through the $[-3,3,0]^*$ position of reciprocal space. Note also that there appears to be very close to a horizontal mirror plane perpendicular to the reflection labeled $[020]^*$ in Fig. 3(a). This implies that the image is taken tilted away from the exact [001] orientation around the $[020]^*$ reciprocal lattice direction and that the direction of the oscillation axis for this image is also close to the $[020]^*$ reciprocal lattice direction.

Under this assumption, Fig. 3(b) shows a drawn to scale Ewald sphere construction of the $h0l^*$ plane of reciprocal space for an incident beam orientation along $[00,-1]$ [the solid Ewald sphere line in Fig. 3(b)] and tilted away from the $[00,-1]$ direction around the $[020]^*$ axis by $\phi\sim 10°$ [the dashed Ewald sphere line in Fig. 3(b)]. [Note that the filled circles in Fig. 3(b) correspond to allowed Bragg reflections of the average *Fm*-3*m* average structure while the open circles are not allowed by the face-centered lattice. There are, however, fcc allowed Bragg reflections immediately above and below which project onto the open circle positions shown.] Given the known wavelength, the $[311]^*$ and $[3,-1,1]^*$ Bragg reflections are then excited, i.e., exactly fall on the Ewald sphere, at $\phi=7.96°$, the $[422]^*$ and $[4,-2,2]^*$ reflections at $\phi=10.28°$, the $[-2,00]^*$ at $\phi=6.00°$ and the $[-2,2,0]^*$ and $[-2,-2,0]^*$ reflections at $\phi=12.07°$. A $\pm 2.5°$ oscillation around an average orientation of ~8.5° would then give rise to the simultaneous excitation of all the Bragg reflections just discussed except for the $[-2,2,0]^*$ and $[-2,-2,0]^*$ reflections which would nonetheless be very close to being excited. Similar considerations have been used to "index" each of the observed oscillation images in Fig. 2.

In Fig. 4(a), for example, the $[1,-1,3]^*$ (and $[-1,1,3]^*$) reflections fall exactly on the Ewald sphere at $\phi=11.05°$ {ϕ defined relative to the $[-2,-2,0]^*$ reciprocal lattice direction, see Fig. 4(b)}, the $[1,-1,1]^*$ and $[-1,1,1]^*$ reflections at $\phi=9.02°$, the $[1,1,-3]^*$ reflection at $\phi=15.26°$ [corresponding to the solid Ewald sphere line in Fig. 4(b)] and the $[002]^*$ reflection at $\phi=6.00°$ [corresponding to the dashed Ewald sphere line in Fig. 4(b)]. A $\pm 2.5°$ oscillation around an average orientation of $\phi\sim 8.5°$ degrees would then give rise to the simultaneous excitation of all of the Bragg reflections just discussed except the $[1,1,-3]^*$ reflection which would nonetheless be very close to being excited. On the other hand, the $[0,2,-2]^*$ and $[2,0,-2]^*$ reflections only fall exactly on the Ewald sphere at $\phi=25.44°$, an angle relatively close to but nonetheless significantly removed from the estimated average orientation of $\phi\sim 8.5°$ [see Fig. 4(b)]. This again requires that the observed diffuse streaking running through "$[2,0,-2]^*$" and "$[0,2,-2]^*$" in Fig. 4(a) arises from a cut through a planar diffuse distribution centered on the true $[2,0,-2]^*$ and $[0,2,-2]$ Bragg reflections [see Fig. 5(b)].

Note that each of the images in Fig. 2 show relatively sharp,[21] diffuse streaking, always along directions of reciprocal space perpendicular to one or more of the $\frac{1}{2}\langle 110\rangle$ molecular nearest neighbor-directions of the average structure, e.g., along the $[220]^*$ direction perpendicular to $\frac{1}{2}[-1,1,0]$ in Fig. 2(a) {see also Fig. 3(a) where this $[220]^*$ direction of the diffuse streaking is marked by the doubled headed arrow and the label **q** while the necessarily orthogonal direction of the atomic shifts responsible are labeled by the displacement eigenvector $\mathbf{e}_\mu(\mathbf{q})$ and the single headed arrow}, also along the $[1,-1,1]^*$ direction perpendicular to $\frac{1}{2}[110]$, $\frac{1}{2}[1,0,-2]$, and $\frac{1}{2}[011]$ in Fig. 2(b) and along the $[020]^*$ direction perpendicular to $\frac{1}{2}[101]$ and $\frac{1}{2}[1,0,-1]$ in Fig. 2(c) [and Fig. 2(a)], etc.

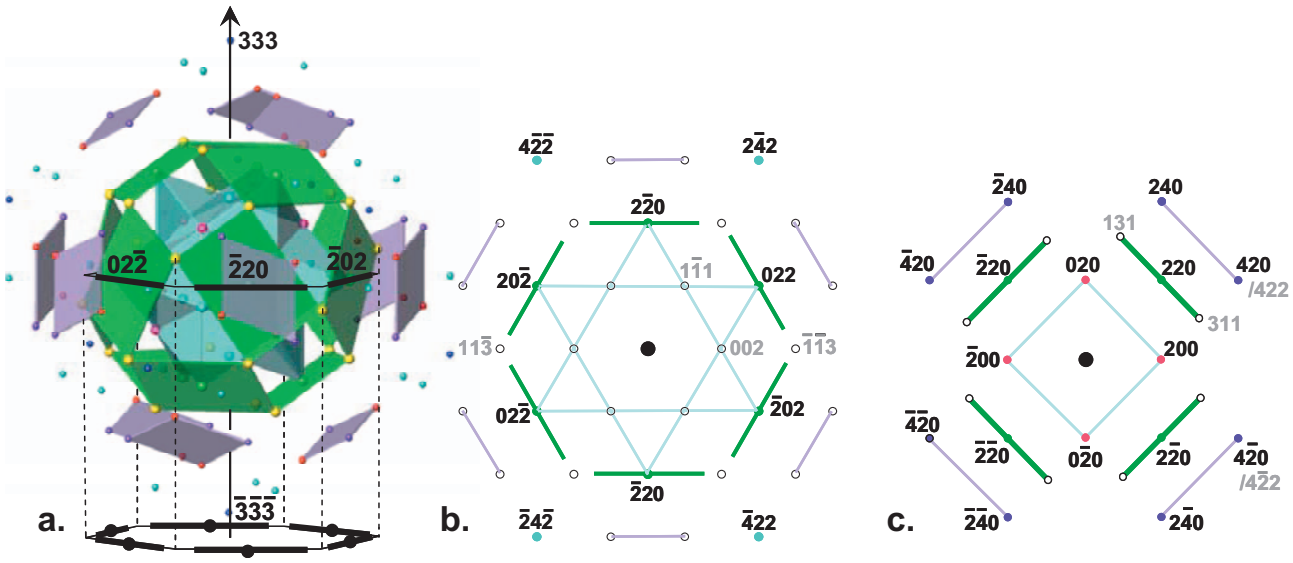

FIG. 5. (Color) (a) A three-dimensional representation of the reciprocal space of α-CBr_4, with the $[111]^*$ reciprocal lattice direction as the vertical axis. The $n=1$, 2, and 3 sheets of $\frac{1}{2}\{1,1,0\}^*$ diffuse are shown as light blue, green, and lavender, respectively. Small colored spheres represent allowed reflections of the fcc lattice ($\langle 200\rangle^*$ fuchsia, $\langle 111\rangle^*$ turquoise, $\langle 220\rangle^*$ green, $\langle 113\rangle^*$ yellow, $\langle 420\rangle^*$ purple, $\langle 331\rangle^*$ red, $\langle 422\rangle^*$ turquoise, and $\langle 333\rangle^*$ dark blue). (b) and (c) Two-dimensional cross sections of the reciprocal space perpendicular to the $[111]^*$ and $[022]^*$ reciprocal lattice directions, respectively. Solid lines represent the observed diffuse and filled circles represent observed reflections in these planes. Open circles representing allowed reflections just above or below the cross section are added to facilitate comparison to the observed images of Fig. 2 and the Ewald constructions in Figs. 3 and 4.

An important aspect of the streaking is that it is *transversely polarized*.[21] By this is meant the experimental observation that the intensity of the diffuse streaking through the allowed average structure Bragg reflections **G** along, e.g., the $\mathbf{q}=\varepsilon[-2,-2,0]^*$, ε continuous, directions of reciprocal space in Fig. 3(a) (see the double-headed white arrow therein) is strongly observed in the vicinity of the $\mathbf{G}=[-2,2,0]^*$ reflection but is completely absent in the vicinity of the $\mathbf{G}=[-2,-2,0]^*$ reflection and vice versa. From the diffraction point of view, this "extinction condition" in the diffuse scattering requires that the displacement eigenvectors $\mathbf{e}_\mu(\mathbf{q})$ [see Fig. 3(a)] and hence atomic displacements $[\mathbf{u}_\mu(\mathbf{r}_\mu+\mathbf{t})=\Sigma_\mathbf{q}\mathbf{e}_\mu(\mathbf{q})\exp 2\pi i\mathbf{q}(\mathbf{r}_\mu+\mathbf{t})$; $\mathbf{r}_\mu$ the position of the μth atom in the $\mathbf{t}$th unit cell, $\mathbf{u}_\mu(\mathbf{r}_\mu+\mathbf{t})$ the displacement of the μth atom at position $\mathbf{r}_\mu+\mathbf{t}$] responsible for the observed diffuse streaking must necessarily occur largely perpendicular to the direction of the streaking itself, i.e., the diffuse streaking along the $\varepsilon[-2,-2,0]^*$, ε continuous, direction of reciprocal space in Fig. 3(a) arises from correlated atomic displacements along the molecular nearest neighbor $\frac{1}{2}[-1,1,0]$ direction of real space and vice versa. For more details of the modulated structure notation used above, see, e.g., Ref. 21.

The observed images can thus only be understood in terms of Ewald sphere cuts through transversely polarized, $\frac{1}{2}\{-1,1,0\}^*$ sheets of diffuse scattering running through all allowed average structure Bragg reflections (see Fig. 5). These $\frac{1}{2}\{-1,1,0\}^*$ sheets of diffuse scattering are quite characteristic of the plastic phase of CBr_4. Experimentally, by far the strongest of these $\frac{1}{2}\{-1,1,0\}^*$ sheets of diffuse intensity are the second order ($n=2$) sheets running through the family of twelve $\langle 220\rangle^*$ type Bragg reflections (see green sheets and lines in Fig. 5). These collectively form a small rhombihexahedron [see Fig. 5(a)] about the origin of reciprocal space with the twelve rectangular faces thereof each centered on a particular $\langle 220\rangle^*$ Bragg reflection. It is these $n=2$ sheets of diffuse scattering that, when orientationally averaged, give rise to the "…intense and rather broad diffuse scattering…observed near 2 $Å^{-1}$"…which could not be fitted over "…the range …$2.0\leqslant Q\leqslant\sim 3.0$ $Å^{-1}$…."[1] Note that the lines in reciprocal space where neighboring $\frac{1}{2}\{110\}^*$ sheets of diffuse intensity intersect and hence appear stronger in intensity are along the $\langle 111\rangle^*$ directions of reciprocal space. This explains the "…cigar-shaped (diffuse) intensity contours elongated along the $\langle 111\rangle^*$ directions…" reported in Ref. 16. Much weaker first ($n=1$) and third ($n=3$) order $\frac{1}{2}\{110\}^*$ sheets (blue and lavender, respectively, in Fig. 5) running through Bragg reflections such as $[200]^*$, $[020]^*$, and $[111]^*$ in the case of the first-order sheets and $[-2,4,0]^*$ and $[-4,2,0]^*$ in the case of the third-order sheets are also detectable experimentally, but only just (see Fig. 2).

The observed diffuse distribution is reminiscent of paracrystalline lattices; in particular paracrystalline lattices exhibiting strong longitudinal correlation (see, e.g., Fig. 6.5 of Ref. 22). The transverse polarized nature of the diffuse distribution necessitates a displacive origin, in particular correlated longitudinal rigid body displacements primarily along the molecular nearest neighbor $\frac{1}{2}\langle 110\rangle$ directions of real space. Such molecular displacements can only arise as a result of van der Waals interactions between neighboring CBr_4 molecules induced by their local relative orientations and, in particular, by the distribution of nearest neighbor intermolecular Br-Br separation distances.

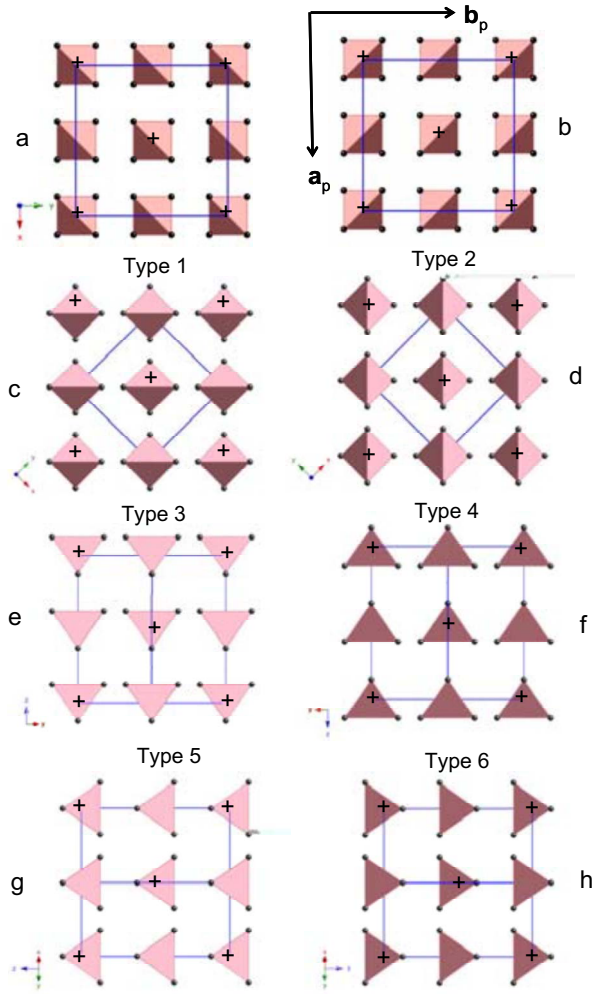

FIG. 6. (Color online) Various high symmetry ways of orienting individual tetrahedra within the *Fm*-3*m* average structure unit cell of α-CBr_4 (tetrahedra on the front face of the cell are indicated with a +). (a) and (b) show long-range ordered, symmetry equivalent *F*-43*m* ($\mathbf{a}=\mathbf{a}_p$, $\mathbf{b}=\mathbf{b}_p$, $\mathbf{c}=\mathbf{c}_p$, *p* for the *Fm*-3*m* parent) structures. (c)–(h) show the six symmetry equivalent ways of orienting the next highest symmetry, fully ordered *I*−42*m* ($\mathbf{a}'=\frac{1}{2}(\mathbf{a}_p+\mathbf{b}_p)$, $b'=\frac{1}{2}(-\mathbf{a}_p+\mathbf{b}_p)$, $\mathbf{c}'=\mathbf{c}_p$) option. Note that (c) is obtained from (a) by rotating the tetrahedra by 45° around the $\mathbf{c}_p$ direction.

III. THEORETICAL CONSIDERATIONS

In order to avoid far too short intermolecular Br-Br separation distances, it has long been recognized that nearest neighboring CBr_4 molecules should never simultaneously bring Br atoms into the vicinity of the $\frac{1}{2}\langle 110\rangle$ direction joining the two molecules[12] as, for example, occurs in the case of the two long range ordered, symmetry equivalent *F*-43*m* ($\mathbf{a}=\mathbf{a}_p$, $\mathbf{b}=\mathbf{b}_p$, $\mathbf{c}=\mathbf{c}_p$, *p* for parent) structures shown in Figs. 6(a) and 6(b). In each of these "structures," the −43*m* (T_d) point group symmetry of the individual tetrahedra are aligned with the local $m3m=i-43m$ site symmetry of the *Fm*3*m* average structure so that each C-Br bond points along a particular $\langle 111\rangle$ direction. There are two ways of orienting the individual CBr_4 tetrahedra on each site, related by an inversion center through the central C atom. In both the structures, very short intermolecular $d_{\text{Br-Br}}$ distances of 3.113 Å, much shorter than the intermolecular Br-Br van der Waal's radius of ~3.78 Å, exist along all twelve $\frac{1}{2}\langle 110\rangle$ directions simultaneously so that they are not plausible as resultant, or even local, structures without very substantial local displacive and/or orientational relaxations. Basically the CBr_4 molecules would need to push each other apart ~0.67 Å along all twelve $\frac{1}{2}\langle 110\rangle$ directions simultaneously, i.e., the unit cell would expand from ~8.82 to ~10.71 Å, if the pattern of tetrahedral orientations shown in Figs. 6(a) and 6(b) were to be maintained. That these relative orientations are not plausible appears to be consistent with the C-Br orientational distribution function (ODF) determined from the average structure refinement of α-CBr_4 by More *et al.*[11] (see Fig. 2 therein; see also Refs. 9, 12, 16, and 17) which exhibits clear minima for C-Br bonds pointing along the $\langle 111\rangle$ directions.

The next highest symmetry, fully ordered option is to rotate the tetrahedra of Fig. 6(a) by 45° around the $\mathbf{c}_p$ direction giving rise to a resultant structure of *I*−42*m* space group symmetry with $\mathbf{a}'=\frac{1}{2}(\mathbf{a}_p+\mathbf{b}_p)$, $\mathbf{b}'=\frac{1}{2}(-\mathbf{a}_p+\mathbf{b}_p)$, $\mathbf{c}'=\mathbf{c}_p$ [where $a_p=b_p=c_p\sim 8.82-8.85$ Å; see Fig. 6(c)]. The local molecular site symmetry is then −42*m* so that there are six symmetry equivalent tetrahedral orientations as shown in Figs. 6(c)–6(h) respectively. In these symmetry equivalent *I*−42*m* structures, the shortest intermolecular $d_{\text{Br-Br}}$ is 3.924 Å, i.e., only slightly larger than twice the Br van der Waals radius. Note that the C-Br bonds in these *I*−42*m* structures point along $\langle 0,0.1252\sqrt{2},0.1252\rangle$ directions, oriented at 9.736° to the local $\langle 011\rangle$ directions. The C-Br ODF of α-CBr_4 initially determined by More[11] (see Fig. 2 therein) and subsequently confirmed by others (see Refs. 6, 16, and 17) exhibits clear maxima along the twelve $\langle 110\rangle$ directions but with significant tetrahedral librational broadening towards the local $\langle 0,0.1252\sqrt{2},0.1252\rangle$ and $\langle 0,0.1252,0.1252\sqrt{2}\rangle$ directions. (Note these are related by a mirror plane such that there are only six molecular orientations determined by the twelve $\langle 110\rangle$ directions.) This strongly suggests that the most common local orientations of the CBr_4 tetrahedra are the six orientations shown in Figs. 6(c)–6(h).

A fit to the experimental Bragg diffraction data using a Frenkel model with only these six local molecular orientations allowed, however, does not provide an adequate description of the orientational disorder in the plastic phase of CBr_4.[9,11,12,14–17] Nonetheless, it remains the simplest and most plausible starting model for qualitatively understanding the origin of the structured diffuse scattering characteristic of the plastic phase of CBr_4, the aim of the current contribution. Under the assumption that each tetrahedron is locally in one or other of the six orientations shown in Figs. 6(c)–6(h), the question becomes the following: What is the nature of the nearest-neighbor intermolecular orientational and/or displacive correlations? That is, if one particular CBr_4 molecule is locally in one or other of the six orientations shown in Figs. 6(c)–6(h), what are the implications for the orientation and positioning of the nearest neighboring CBr_4 molecules?

IV. MONTE CARLO SIMULATIONS

In order to obtain insight into the structural origin of the observed diffuse distribution, Monte Carlo simulation, and

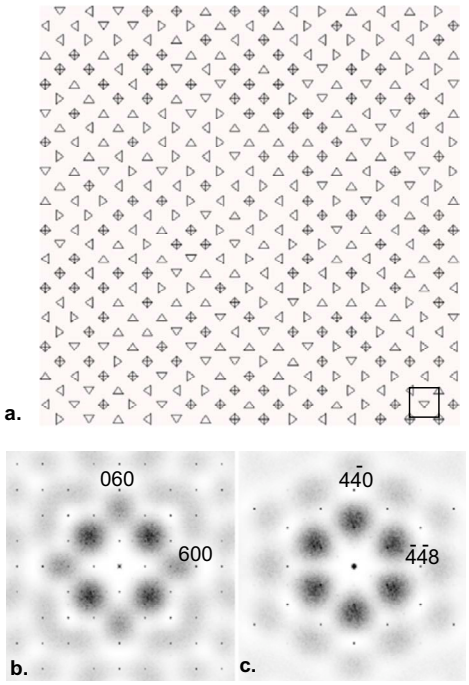

FIG. 7. (Color online) (a) A single layer, unit cell thick portion of a random CBr_4 molecular distribution in projection along an $\langle 001\rangle_p$ direction (the tetrahedra have been drawn smaller than they actually are for the purposes of clarity). The C atom of each molecule is anchored to the fcc sites of the *Fm*-3*m* average structure while each molecule is assumed to be in one or other of the six possible molecular orientations shown in Figs. 6(c)–6(h) to h. The corresponding Fourier transformed reciprocal space corresponding to this random real space distribution is shown in (b) along the [001] direction and (c) along the [111] direction.

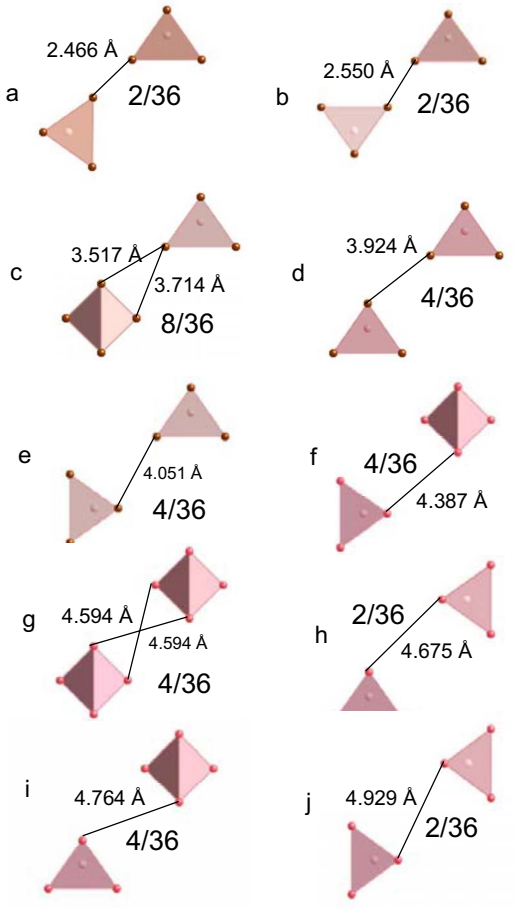

FIG. 8. (Color online) Representation of the 10 (nonsymmetry equivalent) distinct nearest-neighbor molecular configurations, along with their frequency of occurrence in the case of a random distribution. The shortest intermolecular Br-Br separations distances for these 10 distinct configurations are also shown. An equivalent set of interactions occurs along all twelve such $\frac{1}{2}\langle 110\rangle_p$ separations surrounding any one particular CBr_4 molecule.

subsequent Fourier transformation has been used to generate real space CBr_4 molecular distributions and their resulting scattering patterns. The simulations were performed using a box comprising $32\times32\times32$ unit cells, each containing four CBr_4 molecules. Figure 7(a), for example, shows a single layer unit cell thick portion of a random CBr_4 molecular distribution in projection along an $\langle 001\rangle_p$ direction (the tetrahedra have been drawn smaller than they actually are for the purposes of clarity in this figure). The C atom of each molecule at this stage is anchored to the fcc sites of the *Fm*-3*m* average structure while each molecule is assumed to be in one or other of the six possible molecular orientations shown in Figs. 6(c)–6(h). The corresponding Fourier transformed reciprocal space corresponding to this random real space orientational distribution is shown in Fig. 7(b) along the [001] direction and in Fig. 7(c) along the [111] direction. Note the presence of strong blobs of diffuse intensity forming a lattice with reciprocal space basis vectors $\sim\langle 2.3,2.3,0\rangle_p^*$.

For a random distribution over six orientations, note that along any one molecular nearest neighbor $\frac{1}{2}\langle 110\rangle$ direction, neighboring CBr_4 molecules separated by $\frac{1}{2}\langle 110\rangle_p$ can have 36 possible configurations—six for molecule 1 and six for molecule 2, giving $6\times6=36$ overall. Careful consideration, however, shows that many of these configurations are symmetry equivalent. There are in fact only 10 (nonsymmetry equivalent) distinct such nearest-neighbor configurations possible and these are shown in Fig. 8 along with their frequency of occurrence in the case of a random distribution. The shortest intermolecular Br-Br separations distances for these 10 distinct configurations are also shown. Note the enormous spread in these shortest intermolecular Br-Br separation distances (2.5–4.9 Å) compared to the ideal distance of ~3.80 Å. An equivalent set of interactions occurs along all twelve such $\frac{1}{2}\langle 110\rangle_p$ separation distances surrounding any one particular CBr_4 molecule.

As a first-order perturbation we censor the random Frenkel model such that all exceedingly short contacts, i.e., less than 3 Å, are removed. Were these shortest contacts of 2.466 and 2.550 Å to be mitigated by displacive relaxation a shift on the order of 1.3 Å would be required [see Figs. 8(a) and 8(b)]. Given the experimental translational Debye-Waller factor $\langle u^2\rangle$ of $(0.60\ \text{Å})^2$ refined via the Frenkel six orientation only model for CBr_4,[16] this is most unrealistic. The two local configurations shown in Figs. 8(a) and 8(b), as well as their symmetry equivalent variants, were therefore systematically removed prior to relaxation. This was achieved via

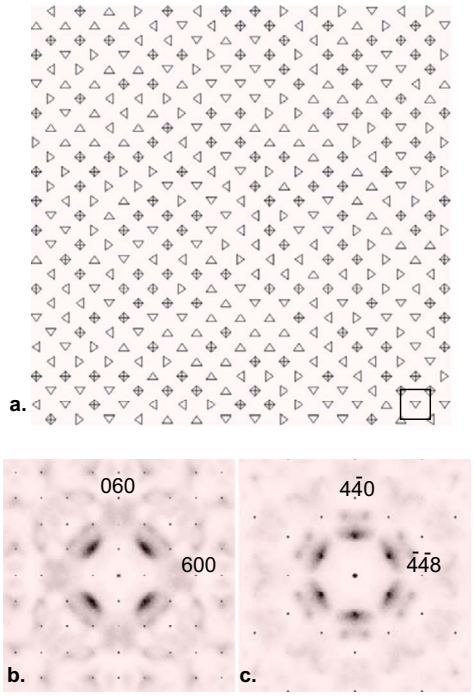

FIG. 9. (Color online) Representation of the real space distribution obtained for a censored Frenkel model after removal of the two local configurations shown in Figs. 8(a) and 8(b) involving Br-Br separation distances of 2.466 and 2.550 Å, respectively, and its corresponding reciprocal space projection along [001] in (b) and along [111] in (c).

Monte Carlo simulation by imposing a strong energy penalty term if either of the two configurations shown in Figs. 8(a) and 8(b) (or any of their symmetry equivalent variants) occurred. The corresponding real space distribution after the removal of these two unphysical local configurations is shown in Fig. 9(a), its corresponding reciprocal space in projection along [001] in Fig. 9(b), and in projection along [111] in Fig. 9(c). Note that the strong blobs of diffuse intensity apparent in Figs. 7(b) and 7(c) have as a result been broken up into more localized diffuse scattering representing the beginnings of discrete planes of diffuse intensity perpendicular to the $\frac{1}{2}\langle 110\rangle$ directions of real space [cf. Fig. 9(b) with Fig. 7(b) and Fig. 9(c) with Fig. 7(c)] just as is observed experimentally [cf. Fig. 9(b) with Fig. 2(a) and Fig. 9(c) with the left-hand side of Fig. 2(b)].

At this stage, given an ideal intermolecular $d_{\text{Br-Br}} \sim 3.80$ Å, local rigid body displacements of the molecular positions away from their perfect fcc lattice sites were introduced in order to minimize the intermolecular Br-Br van der Waals interaction energies. A simple Hooke's law type restoring force along the directions of the shortest intermolecular Br-Br separation distances was thus introduced pulling the molecules closer together if $d_{\text{Br-Br}}$ is >3.80 Å [as, for example, in the Figs. 8(d)–8(j) local configurations] and pushing them further apart if $d_{\text{Br-Br}}$ is <3.80 Å [for example, in the case of the most common local configuration shown in Fig. 8(c)]. While the direction of the shortest intermolecular Br-Br separation distances does not always point along the local $\frac{1}{2}\langle 110\rangle$, the average C-Br orientations point along this direction when the symmetry related variants of the configurations shown in Fig. 8 are taken into account. Thus, average longitudinal displacements of the individual CBr_4 molecules along the nearest neighbor $\frac{1}{2}\langle 110\rangle$ directions to minimize such Br-Br interactions will be induced by such a restoring force in order to minimize the intermolecular Br-Br van der Waals interaction energies. These shifts will clearly be of the right form to explain the experimentally observed transverse polarized diffuse intensity distribution (see Fig. 2).

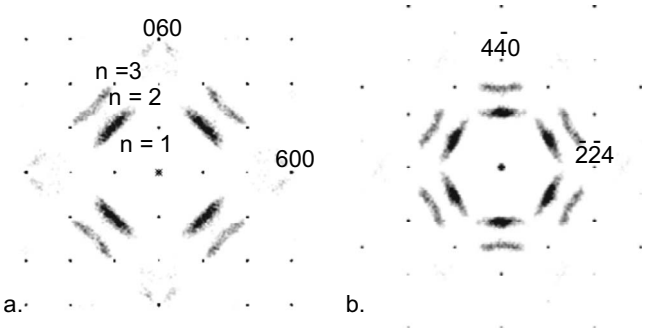

FIG. 10. Calculated diffraction patterns in projection along (a) [100] and (b) [111], respectively, after Monte Carlo relaxation as described in the text.

With the distribution of molecular orientations kept fixed, a sequence of Monte Carlo cycles were then performed to allow the positions of the CBr_4 molecules to relax. 100 cycles of iteration were found sufficient to achieve a configuration that was considered close to fully relaxed. Diffraction patterns were then computed for comparison with the unrelaxed patterns described above. Figures 10(a) and 10(b) show diffraction patterns of the relaxed distributions in projection along [100] and [111], respectively. Comparison with Figs. 9(b) and 9(c) shows that the distortion has had a significant effect on the distribution of intensity in the patterns. The transverse polarized diffuse streaking perpendicular to the $\langle 110\rangle^*$ directions of reciprocal space are now quite marked with by far the strongest such streaking running through the $\langle 220\rangle^*$ Bragg reflections just as is observed experimentally [cf. Fig. 10(a) with Fig. 2(a) and Fig. 10(b) with the left-hand side of Fig. 2(b)]. While the agreement with experiment is not perfect (the weak inner diffuse just visible in Fig. 2, in particular, is not picked up in Fig. 10), it is qualitatively really quite good. We believe the weak inner structured diffuse scattering is not picked up in Fig. 10 because of the assumption that each tetrahedron may only take one or the other of the 6 orientations shown in Figs. 6(c)–6(h), thus ignoring librations of the tetrahedra that obviously also take place. Any such libration would destroy the local mirror symmetry resulting in 12 possible molecular orientations corresponding to the 12 $\langle 110\rangle$ directions.

For the purposes of computational simplicity, we did not allow tetrahedral rotations. This is clearly not an entirely reasonable assumption, given the isotropic rotational Debye-Waller factor of $\langle\omega\rangle^2 = 3 \times 0.05$ rad^2, i.e., $\sqrt{\langle\omega\rangle^2} \sim 0.387$ rad $= 22.2°2$ or 2--> refined via the Frenkel six orientation only model for CBr_4. Nonetheless, given the very significant increase in complexity that would be required to quantitatively model both orientational and displacive degrees of freedom

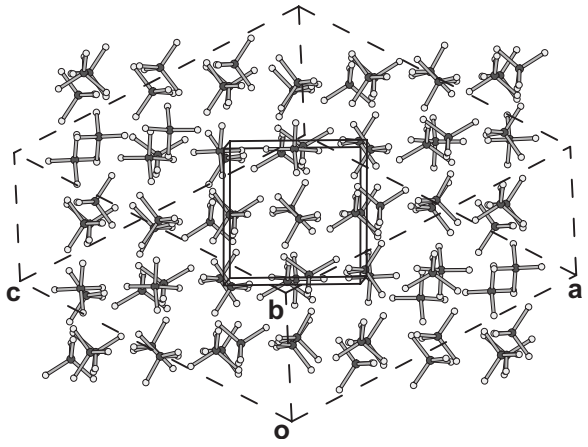

FIG. 11. Ball and stick drawing of the crystal structure of β-CBr_4 oriented so as to emphasize the fcc molecular arrangement. The fcc subcell is indicated with solid lines, whereas the monoclinic cell of the β phase is indicated with dashed lines.

simultaneously as well as the fact that the nonrotated model still captures the essence of the crystal chemistry underlying the observed diffuse scattering (see below), it was considered to be a reasonable price to pay. Possible attractive head-to-tail interactions postulated for the CCl_4 analog[23] could also be considered. But it should be kept in mind that the information available in diffuse patterns is relatively limited. In general, models need to be kept as simple as possible in order to avoid overparametrization. It is clear that the model discussed in this work captures the essential physics of the observed diffuse scattering.

Finally it is interesting to consider how the orientational constraints of this model proposed to describe the plastic crystalline phase relate to the low temperature β phase of CBr_4. More *et al.* describe the relationship between the $C2/c$, monoclinic β phase ($\mathbf{a}=21.43$ Å, $\mathbf{b}=12.12$ Å, $\mathbf{c}=21.02$ Å, and $\beta=110.88°$) and the plastic fcc α phase as $\mathbf{a}=-2\mathbf{a}_p+\mathbf{b}_p-\mathbf{c}_p$, $\mathbf{b}=\mathbf{b}_p+\mathbf{c}_p$, and $\mathbf{c}=2\mathbf{a}_p+\mathbf{b}_p-\mathbf{c}_p$ (thus $\mathbf{a}_p=8.63$ Å, about a 3% contraction from the higher temperature α phase), corresponding to $\mathbf{a}^*=\frac{1}{4}[-1,1,-1]_p^*$, $\mathbf{b}^*=\frac{1}{4}[022]_p^*$, and $\mathbf{c}^*=\frac{1}{4}[1,1,-1]_p^*$.[10] The observed monoclinic angle is only slightly expanded from the 109.47° angle expected for an idealized cell based on a supercell of the fcc α phase. As shown in Fig. 11, the CBr_4 molecules in the β phase reside on approximate fcc sites, each oriented in one of the six symmetry equivalent molecular orientations defined by the $-42m$ site symmetry such that the C-Br bonds approximately lie along the fcc [110] directions. The 36 molecules of the monoclinic cell are distributed with two orientations each adopted by 8 molecules and four orientations each adopted by 5 molecules. Pair-wise intermolecular Br-Br contacts range between 3.6 and 3.9 Å (average 3.85 Å). Thus, the restricted number of molecular orientations and the respective Br-Br distances in the crystal structure of the low temperature β phase provides strong support for the structural constraints imposed in our simulations. The C centering implies that only hkl reflections for which $h+k$ are allowed, i.e., the primitive basis vectors of the reciprocal lattice are $[110]^*=\frac{1}{4}[-1,3,-1]_p^*$, $[1,-1,0]^*=\frac{1}{4}[-1,-1,-3]_p^*$, and $[001]^*=\frac{1}{4}[1,1,-1]_p^*$. Each of these reciprocal space basis vectors is perpendicular to at least one of the molecular nearest neighbor $\frac{1}{2}\langle 110\rangle_p$ real space directions and thus are consistent with the $\mathbf{G}\pm\frac{1}{2}\{110\}^*$ sheets of diffuse intensity we report in the high-temperature phase.

Furthermore, it is remarkable to consider the thermodynamic implications of a simplistic ordering from the above-described model of the plastic crystal to the monoclinic crystalline phase, whereby each molecule must lock into only one of the 6 possible orientations based on the $-42m$ local symmetry if there is no molecular libration, or 12 possible orientations if molecular libration is considered. If the ordering is described as simply going from $W=12$ choices (i.e., *with libration*) to $W=1$ choice for each molecule, to a first approximation, that would mean a drop in entropy of $R\ln(12/1)=20.7$ J/Kmole. Silver and Rudman report a ΔH of 1581 cal/mole at $T=320$ K for the α/β transition.[8] This computes to an experimental $\Delta S=20.6$ J/Kmole. Thus, Frenkel disorder maintaining the local $-42m$ symmetry giving six possible molecular orientations, considered in the simulation reported here accounts, for about 70% of the ΔS of the α-β transition. The remaining ΔS can be attributed to displacive and librational disorder.

V. SUMMARY AND CONCLUSIONS

Time and temperature dependent two-dimensional synchrotron x-ray diffraction data of an *in situ* grown single plastic crystal of CBr_4 provide unprecedented insight as to structure and molecular correlations in this soft condensed material. A highly structured distribution of transverse polarized, quite sharp $\frac{1}{2}\{110\}^*$ sheets of diffuse intensity arising from the large amplitude excitation of individual, transverse optical modes of distortion, has been observed. This intense, highly structured diffuse scattering is shown to arise primarily from the sixfold censored Frenkel disorder and displacive relaxations along the molecular nearest-neighbor $\frac{1}{2}\langle 110\rangle$ real space directions associated with the local relative orientations of the individual CBr_4 tetrahedra. This model confirms that α-CBr_4 is not a rotor phase, although librational motions contribute as a perturbation.

ACKNOWLEDGMENTS

Jonathan C. Hanson is thanked for his support at NSLS Beamline X7B. J.D.M. and J.C.W.F. gratefully acknowledge support from the NSF via the Contracts No. DMR-0305086 and No. DMR-0705190, and R.L.W. and T.R.W. acknowledge the Australian Research Council for funding in the form of ARC Discovery Grants. The research carried out at beam line X7b at BNL-NSLS was supported by Contract No. DE-AC02-98CH10086 with the U.S. DOE, Office of Basic Energy Sciences, Division of Chemical Sciences. The NSLS is supported by the Divisions of Materials and Chemical Sciences of DOE. We also wish to thank the Australian Partnership for Advanced Computing for the provision of computational resources.

[1] L. A. K. Staveley, Annu. Rev. Phys. Chem. **13**, 351 (1962).
[2] L. C. Towle, Science **159**, 629 (1968).
[3] L. C. Towle, Appl. Phys. **2**, 187 (1973).
[4] J. Timmermans, Phys. Chem. Solids **18**, 1 (1961).
[5] C. S. Yoon, J. N. Sherwood, and R. A. Pethrick, J. Chem. Soc., Faraday Trans. 1 **85**, 2867 (1989).
[6] B. Post, Acta Crystallogr. **12**, 349 (1959).
[7] P. Derollez, J. Lefebvre, M. Descamps, W. Press, and H. Grimm, J. Phys.: Condens. Matter **2**, 9975 (1990).
[8] L. Silver and R. Rudman, J. Phys. Chem. **74**, 3134 (1970).
[9] W. Press, J. Chem. Phys. **56**, 2597 (1972).
[10] M. More, F. Baert, and J. Lefebvre, Acta Crystallogr., Sect. B: Struct. Crystallogr. Cryst. Chem. **B33**, 3681 (1977).
[11] M. More, J. Lefebvre, and R. Fouret, Acta Crystallogr., Sect. B: Struct. Crystallogr. Cryst. Chem. **B33**, 3862 (1977).
[12] G. Coulon and M. Descamps, J. Phys. C **13**, 2847 (1980).
[13] G. Coulon, J. Phys. C **15**, 881 (1982).
[14] M. T. Dove, J. Phys. C **19**, 3325 (1986).
[15] M. T. Dove and R. M. Lynden-Bell, J. Phys. C **19**, 3343 (1986).
[16] M. More, J. Lefebvre, B. Hennion, B. M. Powell, and C. M. E. Zeyen, J. Phys. C **13**, 2833 (1980).
[17] G. Dolling, B. M. Powell, and V. F. Sears, Mol. Phys. **37**, 1859 (1979).
[18] Y. Ebisuzaki, J. Cryst. Growth **43**, 648 (1978).
[19] R. E. Dinnebier, B. Hinrichsen, P. Rajiv, and M. Jansen, Rigaku J. **23**, 13 (2006).
[20] P. S. Salmon, Proc. R. Soc. London, Ser. A **445**, 351 (1994).
[21] R. L. Withers, Z. Kristallogr. **220**, 1027 (2005).
[22] T. R. Welberry, *Diffuse X-Ray Scattering and Models of Disorder* (Oxford University Press, Oxford, 2004).
[23] K. Nishikawa, K. Tohji, and Y. Murata, J. Chem. Phys. **74**, 5817 (1981).